

# Highly Efficient Disproportionation of Dihydrogen Peroxide: Synthesis, Structure, and Catalase Activity of Manganese Complexes of the Salicylimidate Ligand

Meenal D. Godbole,<sup>[a]</sup> Michael Kloskowski,<sup>[c]</sup> Ronald Hage,<sup>[a]</sup> Annette Rompel,<sup>[c]</sup>  
Allison M. Mills,<sup>[b]</sup> Anthony L. Spek,<sup>[b]</sup> and Elisabeth Bouwman\*<sup>[a]</sup>

**Keywords:** Catalase / Michaelis–Menten kinetics / Hydrogen peroxide disproportionation / Enzyme mimics / Manganese / Kinetics

Two complexes,  $[\text{Mn}_2(\text{etsalim})_4(\text{Hetsalim})_2](\text{ClO}_4)_2$  (**1**), and  $[\text{Mn}(\text{mesalim})_2(\text{OAc})(\text{MeOH})]\cdot\text{MeOH}$  (**2**), in which Hmesalim and Hetsalim are methyl and ethyl salicylimidate, respectively, have been synthesized, fully characterized by X-ray analyses, magnetic susceptibility, UV/Vis and IR spectroscopy, and their catalase activity has been studied. Complex **1** is dinuclear and shows an Mn–Mn distance of 3.37 Å while complex **2** is mononuclear. Both complexes catalyze the disproportionation of hydrogen peroxide into water and dioxygen; they show very high catalase activity exhibiting saturation kinetics in the presence of NaOH. The rate and turnover number of the catalyzed reaction increase dramatically when a few equivalents of base (NaOH) are added to the reaction mixture. The turnover numbers for hydrogen peroxide disproportionation increase from approximately 200 to more than 1500 per manganese ion in less than 2 min for both com-

plexes after addition of a few equivalents of NaOH. Kinetic studies of the catalyzed reaction performed on the dinuclear complex **1** in the presence of 5 equiv. of NaOH, gives  $k_{\text{cat}} = 807 \text{ s}^{-1} (\pm 16)$  and  $K_{\text{M}} = 0.091 \text{ M} (\pm 0.003)$ . The effective catalytic efficiency is  $k_{\text{cat}}/K_{\text{M}} = 8900 \text{ M}^{-1}\text{s}^{-1}$ . The kinetic parameters of the mononuclear complex **2** in the presence of 5 equiv. of NaOH, are  $k_{\text{cat}} = 190 \text{ s}^{-1} (\pm 4)$  and  $K_{\text{M}} = 0.022 \text{ M} (\pm 0.001)$ . The effective catalytic efficiency is  $k_{\text{cat}}/K_{\text{M}} = 8600 \text{ M}^{-1}\text{s}^{-1}$ . The catalase activity of the mononuclear complex,  $[\text{Mn}(\text{mesalim})_2\text{Cl}]$  (**3**) has also been studied, and it shows turnover numbers that are comparable to those of complex **2**. ESI-MS analyses in deuterated solvents have been used to understand the nature of the active species formed on addition of 5 equiv. of NaOH.

(© Wiley-VCH Verlag GmbH & Co. KGaA, 69451 Weinheim, Germany, 2005)

## Introduction

Manganese is present in the active sites of enzymes, such as superoxide dismutase (SOD), manganese catalase, extradiol dioxygenase, arginase and ribonucleotide reductase, the oxygen-evolving complex (OEC) of photosystem II (PSII), and lipoxigenase.<sup>[1]</sup> The mechanisms of action of these enzymes are very diverse and include oxo atom transfer (SOD, catalase, extradiol dioxygenase), the reduction of ribonucleotides to water and deoxyribonucleotides, the oxidation of thiosulfate to sulfate and the four-electron oxidation of

water to dioxygen in Photosystem II.<sup>[2]</sup> The principal mechanism of defense of living cells makes use of superoxide dismutase or catalase enzymes to protect the cell structure against harmful and reactive oxygen species, such as superoxide radicals or dihydrogen peroxide. In addition to widely distributed heme-type catalases, a second class of relatively rare manganese catalases has been found in three bacteria, *Lactobacillus plantarum*,<sup>[3]</sup> *Thermus thermophilus*,<sup>[4]</sup> and *Thermoleophilium album*.<sup>[5]</sup> A dinuclear active site is present in these Mn-catalases, possessing either a  $\text{Mn}^{\text{II}}-\text{Mn}^{\text{II}}$  or  $\text{Mn}^{\text{III}}-\text{Mn}^{\text{III}}$  dimer bridged by a  $\mu$ -(1,3)-carboxylate from glutamate and two  $\mu$ -oxo bridges from solvent molecules that electronically couple the metal centers. The rate of oxygen evolution by these enzymes is very high, i.e. of the order of  $10^5$  to  $10^6$  molecules per second.<sup>[6]</sup>

There is high interest in understanding the chemistry of dinuclear manganese complexes, as much structural and mechanistic information regarding the activity of the enzyme could be obtained through studies on model complexes.<sup>[7,8]</sup> The interaction of hydrogen peroxide and dioxygen with dinuclear manganese complexes has been studied in detail by various groups using several structural as well

<sup>[a]</sup> Leiden Institute of Chemistry, Gorlaeus Laboratories, Leiden University,  
P. O. Box 9502, 2300 RA Leiden, The Netherlands  
Fax: (internat.) + 31-71-5274550  
E-mail: bouwman@chem.leidenuniv.nl

<sup>[b]</sup> Bijvoet Center for Biomolecular Research, Crystal and Structural Chemistry, Utrecht University,  
The Netherlands

<sup>[c]</sup> Institut für Anorganische und Analytische Chemie, Westfälische Wilhelms-Universität,  
Wilhelm-Klemm-Str. 8, 48149 Münster, Germany

Supporting information for this article is available on the WWW under <http://www.eurjic.org> or from the author.

as functional model complexes.<sup>[9–11]</sup> Interaction of metal complexes of Schiff-base ligands with hydrogen peroxide has been a matter of study for a long time now, for many of these have been shown to be good oxidation catalysts<sup>[12]</sup> or enzyme mimics.<sup>[10,13,14]</sup>

In this paper, we report the synthesis, full characterization and catalase activity of two manganese complexes,  $[\text{Mn}_2(\text{etsalim})_4(\text{Hetsalim})_2](\text{ClO}_4)_2$  (**1**), and  $[\text{Mn}(\text{mesalim})_2(\text{OAc})(\text{MeOH})]\cdot\text{MeOH}$  (**2**), in which Hmesalim and Hetsalim are methyl and ethyl salicylimidate, respectively (shown in Figure 1). We also report the catalase studies on the complex  $[\text{Mn}(\text{mesalim})_2\text{Cl}]$  (**3**), the crystal structure of which has been recently reported.<sup>[15]</sup> In addition, a comparison of the structural and spectroscopic characteristics of the three complexes is made. The Hmesalim ligand is commonly used in organic syntheses as a precursor for several other ligands, such as oxazolines.<sup>[16]</sup> The transition-metal coordination chemistry of this simple ligand is, however, completely unexplored.



Figure 1. The ligands Hmesalim and Hetsalim

## Results and Discussion

### Synthetic Aspects

The ligand Hmesalim has been known for over 30 years and is commonly used as a precursor for the synthesis of heterocyclic ligands. Surprisingly, it has very rarely been used in transition metal chemistry. The coordination chemistry of this ligand, however, appears to be very rich.<sup>[17]</sup> Reaction of  $\text{Mn}(\text{ClO}_4)_2$  with Hmesalim in ethanol unexpectedly results in the formation of the dinuclear, phenoxo bridged complex **1**, in which the methoxy group on the ligand is exchanged with the solvent ethoxy group. ESI-MS analyses of a solution of the ligand Hmesalim in ethanol shows two peaks, one for Hmesalim and another for Hetsalim, indicating that the presence of a Lewis acid is not necessary for solvolysis to occur. The complex **1** was synthesized by initially dissolving the Hmesalim ligand in ethanol, thus, in fact by the reaction of the manganese salt with Hetsalim formed (in situ). The mesalim-analog of **1** might also be formed in the solution but complex **1** is the sole product isolated from the reaction mixture. When the reaction is performed in methanol a green product is isolated, which has an IR spectrum similar to that of the complex **1**, but crystals good enough for structure determination could not be obtained and the product did not give good elemental analyses. The synthesis of complex **2** is more complicated. The recrystallization of a concentrated solution of the reaction mixture, by slow evaporation or ether diffusion, gave the complex **2** in pure form. Recrystallization of a dilute

solution led to the formation of several polynuclear manganese clusters over time, thus making the isolation of this pure mononuclear compound difficult. In fact two novel clusters, a hexanuclear cluster with an interesting double-cubane structure, and another octanuclear cluster have been isolated and crystallographically characterized after attempts at recrystallization of the mononuclear complex **2**.<sup>[17]</sup>

### Description of the Crystal Structures

The X-ray structures of the two new manganese complexes,  $[\text{Mn}_2(\text{etsalim})_4(\text{Hetsalim})_2](\text{ClO}_4)_2$  (**1**), and  $[\text{Mn}(\text{mesalim})_2(\text{OAc})(\text{MeOH})]$  (**2**) have been determined. Numerical data and details of the data collection and refinement are presented in Table 1.

Table 1. Crystallographic data for complexes,  $[\text{Mn}_2(\text{etsalim})_4(\text{Hetsalim})_2](\text{ClO}_4)_2$  (**1**), and  $[\text{Mn}(\text{mesalim})_2(\text{OAc})(\text{MeOH})]\cdot\text{MeOH}$  (**2**·MeOH)

	<b>1</b>	<b>2</b> ·MeOH
Empirical formula	C <sub>54</sub> H <sub>62</sub> Cl <sub>2</sub> Mn <sub>2</sub> N <sub>6</sub> O <sub>20</sub>	C <sub>20</sub> H <sub>27</sub> MnN <sub>2</sub> O <sub>8</sub>
Formula mass	1295.88	478.38
<i>a</i> [Å]	10.7886(2)	30.5140(7)
<i>b</i> [Å]	11.7621(2)	30.5140(7)
<i>c</i> [Å]	11.9448(3)	12.3108(4)
<i>a</i> [°]	105.827(1)	90
<i>β</i> [°]	92.536(1)	90
<i>γ</i> [°]	100.032(1)	120
<i>V</i> [Å <sup>3</sup> ]	1429.24(5)	9926.9(5)
<i>Z</i>	1	18
Space group	<i>P</i> $\bar{1}$	<i>R</i> $\bar{3}$
Crystal system	triclinic	rhombohedral
$\rho_{\text{calcd.}}$ [g/cm <sup>3</sup> ]	1.506	1.440
<i>T</i> [K]	150	150
$\mu$ [cm <sup>-1</sup> ]	6.17	6.47
<i>R</i> , <i>wR2</i>	0.044, 0.1029	0.0408, 0.109
<i>S</i>	1.03	1.04

A PLUTON projection of the dinuclear complex **1** is shown in Figure 2. Selected bond lengths and angles are given in Table 2. The molecule is located on an inversion center. Each manganese(II) ion is bound by four different etsalim ligands, in a distorted octahedral N<sub>2</sub>O<sub>4</sub> geometry. Two *trans*-chelating ligands, one of which participates in a  $\mu$ -phenoxo bridge to the other manganese center, form the equatorial plane of the octahedron. One axial site is occupied by the phenolate oxygen atom of a terminally binding ligand and the other by bridging phenolate oxygen from the symmetry-related manganese center.

The Mn–O and Mn–N distances are comparable to other Mn<sup>III</sup> complexes of this type that are known in the literature.<sup>[18]</sup> The axial Mn–O(57) and Mn–O(17a) distances are considerably longer (0.2–0.4 Å) than the Mn–O(phenolate) distances in the equatorial plane. There are two  $\mu$ -phenoxo bridges in the dinuclear core, separating the two manganese ions at a distance of 3.3705(5) Å. This distance is within the normal range of phenoxo-bridged Mn<sup>III</sup> complexes.<sup>[18]</sup> The Mn(1)–O(17)–Mn(1a) angle of 103.99(6)° is also similar to those in Mn<sup>III</sup>-salen com-

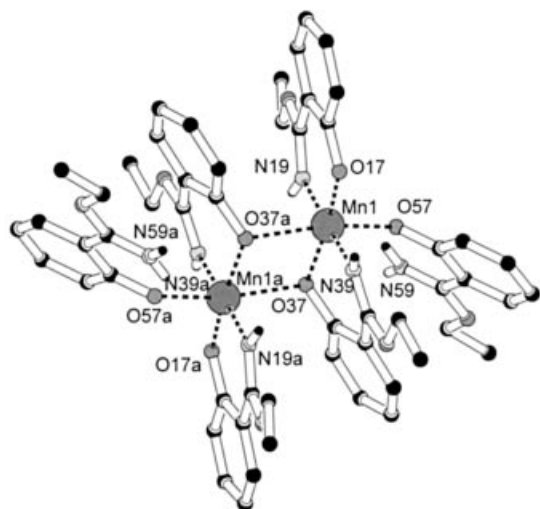


Figure 2. PLUTON projection of the complex  $[\text{Mn}_2(\text{etsalim})_4(\text{Hetsalim})_2]^{2+}$  cation in complex **1**; hydrogen atoms, except those attached to the nitrogen atoms, are omitted for clarity

Table 2. Selected bond lengths [ $\text{\AA}$ ] and angles [ $^\circ$ ] for **1**; symmetry code: a)  $1 - x, -y, 2 - z$

Distance		Angle	
Mn(1)–N(19)	1.9927(17)	Mn(1)–O(17)–Mn(1a)	103.99(6)
Mn(1)–N(39)	2.0005(18)	O(17)–Mn(1)–O(37)	168.99(7)
Mn(1)–O(17)	1.9133(15)	O(17)–Mn(1)–O(57)	90.07(6)
Mn(1)–O(37)	1.8487(15)	O(17)–Mn(1)–N(19)	87.94(7)
Mn(1)–O(57)	2.1284(16)	O(17)–Mn(1)–N(39)	94.33(7)
Mn(1)–O(17a)	2.3507(15)	O(37)–Mn(1)–O(57)	100.31(7)
		O(37)–Mn(1)–N(19)	87.73(7)
		O(37)–Mn(1)–N(39)	89.97(7)
		N(19)–Mn(1)–O(57)	93.70(7)
		N(39)–Mn(1)–O(17a)	90.84(6)
		O(17a)–Mn(1)–O(37)	93.83(6)
		O(57)–Mn(1)–N(19)	93.70(7)
		O(57)–Mn(1)–N(39)	86.65(7)
		O(17a)–Mn(1)–O(57)	165.64(6)
		N(19)–Mn(1)–N(39)	177.70(8)
		O(17a)–Mn(1)–N(19)	89.37(6)

plexes.<sup>[18]</sup> Protonation of the imine nitrogen atoms on the two terminal ligands leaves two positive charges on the complex that are balanced by two perchlorate ions present in the crystal lattice. Each of the imine groups is involved in hydrogen bonding with perchlorate ions in the crystal lattice. The free imine group of the terminal ligand participates in an additional intramolecular hydrogen bond with the coordinated phenolate oxygen atom of the same ligand. (Table 4) (see Figure 1 in the Supporting Information; for Supporting Information see also the footnote on the first page of this article).

A PLUTON projection of the mononuclear complex **2** is shown in Figure 3. Selected bond lengths and angles are given in Table 3. The manganese(III) ion has a distorted octahedral  $\text{N}_2\text{O}_4$  coordination environment. Two chelating mesalim ligand molecules are bound to the metal atom, *cis*

to each other in a square plane. A methanol and a monodentate acetate molecule occupy the two remaining apical positions and complete the octahedron. The Mn–N and Mn–O distances involving the mesalim ligand are slightly longer than those in the complex  $[\text{Mn}(\text{mesalim})_2\text{Cl}]$  (**3**),<sup>[15]</sup> perhaps because the ligands are involved in extensive hydrogen bonding interactions. A PLUTON view of the hydrogen bonding in the crystal lattice is shown in Figure 4, and geometric parameters for the intermolecular hydrogen bonding interactions are listed in Table 4. The complex molecules are paired in a head-to-tail arrangement to form a dimer. Both oxygen atoms from the monodentate acetate ion of each complex molecule form bifurcated hydrogen bonds to each of the two *cis*-imine nitrogen atoms on the neighboring complex molecule and vice versa. Thus, the axially coordinated acetate molecule seems to enforce a *cis* coordination of the mesalim ligands to allow strong hydrogen bonding. The non-coordinated acetate oxygen atom of each complex molecule forms an additional hydrogen bond to the methanol molecule of a neighboring dimer and vice versa. The metal complex cocrystallizes with one independent molecule of methanol. The methanol solvent molecule undergoes intermolecular hydrogen bonding with itself, forming a six-membered ring. A view down the  $[001]$  direction of  $2 \cdot \text{MeOH}$  is presented in Figure 5.

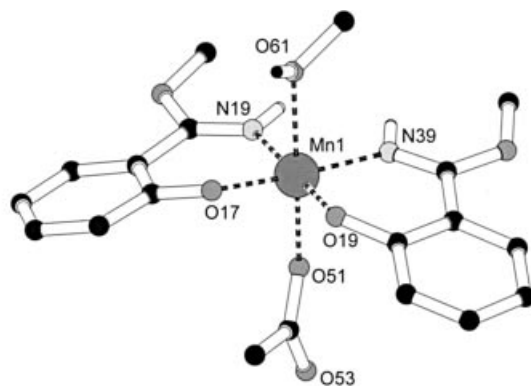


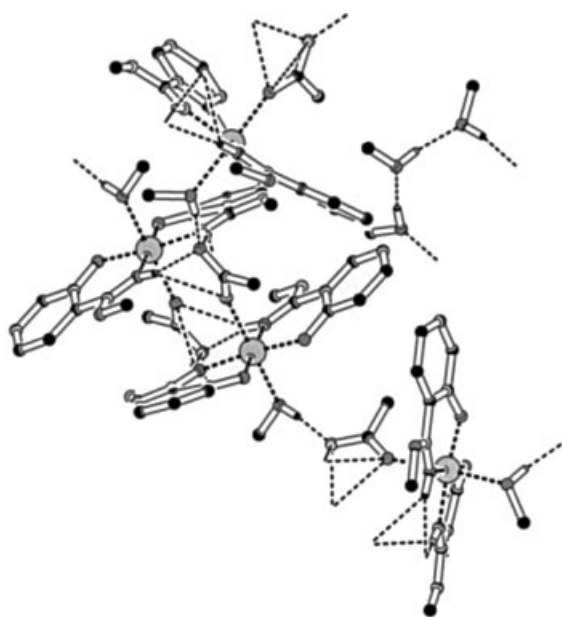
Figure 3. PLUTON projection of  $[\text{Mn}(\text{mesalim})_2(\text{OAc})(\text{MeOH})]$  (**2**); hydrogen atoms except those attached to nitrogen atoms and methanol are omitted for clarity

### Spectroscopic Studies

Complexes **1** and **2** display ligand field bands that are very similar in position. The molar extinction coefficients of **1** are, however, approximately the double of those of absorption intensities of the mononuclear complex **2** because of the presence of two manganese centers and six ligands. In both complexes the peak at 304 nm is assigned to  $\pi\text{-}\pi^*$  transitions within the ligands, because of its high intensity ( $> 10^4 \text{ M}^{-1}\text{cm}^{-1}$ ). The high-intensity band at 357 nm and shoulder at 418 nm can be assigned to the LMCT transition from the phenoxo oxygen to  $\text{Mn}^{\text{III}}$ .<sup>[19–21]</sup> The low-intensity peak at 567 nm ( $\epsilon = 277 \text{ M}^{-1}\text{cm}^{-1}$  in the mononuclear complex and  $\epsilon = 400 \text{ M}^{-1}\text{cm}^{-1}$  in the dinuclear complex) can be assigned to a d-d transition.<sup>[19]</sup> As the position of this

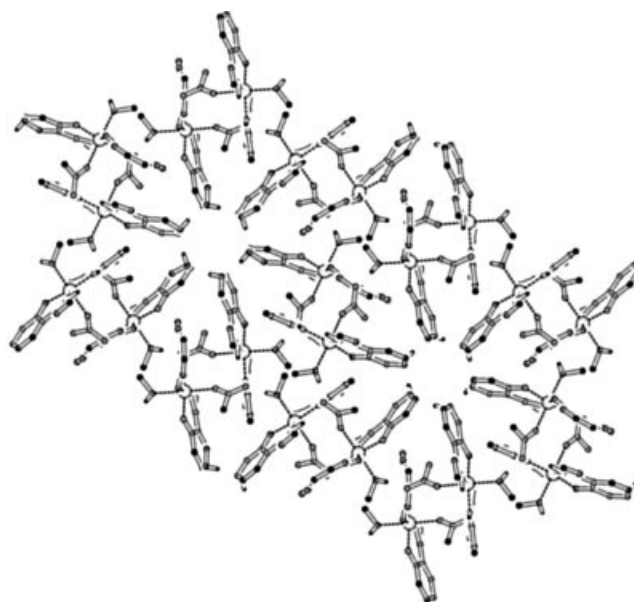
Table 3. Selected bond lengths [Å] and angles [°] for 2·MeOH

Distance		Angle	
Mn(1)–N(19)	2.007(2)	O(17)–Mn(1)–O(37)	88.70(7)
Mn(1)–N(39)	2.018(2)	O(17)–Mn(1)–O(51)	95.50(8)
Mn(1)–O(17)	1.8914(17)	O(17)–Mn(1)–O(61)	87.05(8)
Mn(1)–O(37)	1.8850(17)	O(17)–Mn(1)–N(19)	89.68(8)
Mn(1)–O(51)	2.1535(18)	O(17)–Mn(1)–N(39)	174.09(10)
Mn(1)–O(61)	2.2698(18)	O(37)–Mn(1)–O(51)	91.53(9)
		O(37)–Mn(1)–O(61)	94.71(9)
		O(37)–Mn(1)–N(19)	178.12(9)
		O(37)–Mn(1)–N(39)	88.97(8)
		O(51)–Mn(1)–O(61)	173.32(7)
		O(51)–Mn(1)–N(19)	89.56(9)
		O(51)–Mn(1)–N(39)	89.99(9)
		O(61)–Mn(1)–N(19)	84.27(9)
		O(61)–Mn(1)–N(39)	87.73(9)
		N(19)–Mn(1)–N(39)	92.56(9)

Figure 4. PLUTON projection of hydrogen bonding in [Mn(mesalim)<sub>2</sub>(OAc)(MeOH)] (2)

band is independent of the anions,<sup>[15]</sup> it can be assigned to the  $d_{xy} \rightarrow d_{x^2-y^2}$  transition.<sup>[19]</sup> In addition to these bands complex **1** also shows a weak absorption at 976 nm ( $\epsilon = 76 \text{ M}^{-1}\text{cm}^{-1}$ ). A band similar to this has also been reported for the dinuclear complex,  $[\text{Mn}_2\text{O}(\text{O}_2\text{CCH}_3)_2(\text{tacn})_2]^{2+}$ , which has a band at 990 nm ( $\epsilon = 28 \text{ M}^{-1}\text{cm}^{-1}$ ).<sup>[22]</sup> This band can be compared to that of manganese catalase from *Thermus thermophilus* also, where a broad tail is observed going into the near-IR region and a d-d transition is centered at approximately 492 nm.<sup>[23]</sup>

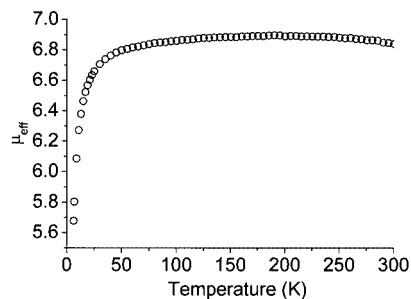
The IR spectrum of the free ligand displays a broad peak characteristic of the phenol O–H at  $2538 \text{ cm}^{-1}$ . The imine C=N frequency in the free ligand occurs at  $1653 \text{ cm}^{-1}$  and shifts to  $1615\text{--}1605 \text{ cm}^{-1}$  after complexation to Mn in all complexes. The presence of the perchlorate anion in the complex **1** is confirmed by a very intense band at  $1088$

Figure 5. Projection of part of the crystal structure of **2** down the [001] axis; solvent methanol molecules joined in six-membered hydrogen-bonded rings around the threefold inversion axesTable 4. Hydrogen bond details (distances [Å] and angles [°]) for compounds **1** and 2·MeOH; symmetry codes: a)  $-x, -y, 1-z$ ; b)  $1-x, -y, 1-z$ ; c)  $1/3-x, 2/3-y, 2/3-z$ ; d)  $x-y, x, 1-z$ ; e)  $y, -x+y, -z$ 

Donor (D)–H...Acceptor (A) <sup>[a]</sup>	H...A	D...A	D–H...A
<b>1</b>			
N19–H19...O4a	2.45	3.251(3)	152
N39–H39...O3b	2.28	3.131(3)	162
N59–H59A...O5b	2.15	2.987(3)	159
N59–H59B...O57	1.87	2.567(3)	135
<b>2·MeOH</b>			
N19–H19...O51c	2.57	3.210(3)	130
N19–H19...O53c	2.19	3.044(3)	164
N39–H39...O51c	2.47	3.098(3)	129
N39–H39...O53c	2.28	3.126(3)	162
O61–H61...O53d	1.77(3)	2.616(3)	174(3)
O71–H71...O71e	1.88	2.711(4)	169

<sup>[a]</sup> D–H distances are all constrained to  $0.88 \text{ Å}$  except for O61–H61...O53d and O71–H71...O71e that is  $0.84 \text{ Å}$ .

$\text{cm}^{-1}$ . For both complexes **1** and **2**, N–H stretching vibrations are seen at  $3278 \text{ cm}^{-1}$  and  $3175 \text{ cm}^{-1}$ , respectively. For complex **2**, the acetate vibrating modes could not be

Figure 6. Variable-temperature magnetic susceptibility of complex **1**

exactly assigned because several ligand peaks were present in the region. Room temperature magnetic measurements for all complexes are consistent with the presence of  $\text{Mn}^{\text{III}}$ . Variable temperature magnetic susceptibility measurements were performed for complex **1**, and a plot of the effective magnetic moment versus temperature is shown in Figure 6. The steep decrease in magnetic moment at temperatures below 25 K is due to the zero-field splitting typical for  $\text{Mn}^{\text{III}}$  ions.

### Catalase Activity and Kinetics

The catalase activity of three complexes  $[\text{Mn}_2(\text{etsalim})_4(\text{Hetsalim})_2](\text{ClO}_4)_2$  (**1**),  $[\text{Mn}(\text{mesalim})_2(\text{OAc})(\text{MeOH})]\cdot\text{MeOH}$  (**2**· $\text{MeOH}$ ) and  $[\text{Mn}(\text{mesalim})_2\text{Cl}]$  (**3**)<sup>[15]</sup> has been studied, both in the presence and absence of different amounts of sodium hydroxide (NaOH), because the enhancing effect of small amounts of NaOH on catalase activity has been reported recently.<sup>[24]</sup> Addition of hydrogen peroxide to alcoholic solutions of the new manganese–mesalim and –etsalim complexes leads to vigorous evolution of dioxygen. The green solutions of the complexes turn brown when NaOH is added, and when subsequently  $\text{H}_2\text{O}_2$  is added to these alkaline solutions, the reaction mixture turns from brown to colorless, with a brown precipitate, meanwhile showing even more vigorous evolution of dioxygen. The total conversion of hydrogen peroxide disproportionation was measured using a manometric method, while the kinetic studies were performed on the basis of fluorescence quenching using an oxygen sensor.<sup>[11,25]</sup> The total catalytic activity as well as the rate of the reaction increases significantly when a few equivalents of NaOH are added. In Table 5 the turnover numbers for the disproportionation of  $\text{H}_2\text{O}_2$  by the manganese complexes in the presence and absence of NaOH are compared. It is interesting to note that the mononuclear complexes **2** and **3** also show very high catalase activity and reach comparable turnovers of manganese ion per minute (TON  $\approx$  1500) as the dinuclear complex. In fact, the mononuclear complex **2** shows even higher turnover per manganese ion (1800) than the dinuclear complex **1** (1575). The complexes **2** and **3** show very similar catalase activity, possibly indicating that a similar active species is formed. A plot of the percentage conversion of hydrogen peroxide for complex **1** followed in time as a function of the amount of NaOH that is added is shown in Figure 7. The highest initial rate is observed when 5 equiv. of NaOH are added. When 7 equiv. of NaOH are added, the initial rate is lower than for 5 equiv. of NaOH, but the catalyst is active for a longer time, which results in turnover numbers above 3000 for complex **1** and 5 equiv. of NaOH in less than 2 min. A similar observation of a breakpoint in the rate acceleration when 5 equiv. of NaOH are added has been reported previously.<sup>[24]</sup> When more hydrogen peroxide is added at the end of a reaction, only very slow evolution of dioxygen occurs, indicating that the catalyst has decomposed. The reactions reach completion within the first two minutes. No lag phase is observed for the reaction with or without addition of NaOH. The blank reaction performed with  $\text{Mn}^{\text{II}}$  perchlorate yields only 190

turnover numbers in total after 4 min even in the presence of 5–6 equiv. of NaOH, while no reaction is observed in the absence of NaOH.

The kinetics for the catalase reaction of the two complexes **1** and **2** has been studied. Figure 8 shows saturation kinetics for the two complexes **1** and **2** in combination with 5 equiv. of NaOH each. Figure 9 shows Lineweaver–Burk plots of the two systems, demonstrating a linear relationship between the rate of substrate disproportionation and substrate concentration for both systems, from which the Michaelis–Menten parameters can be extracted. For the system consisting of complex **1** and 5 equiv. of NaOH,  $k_{\text{cat}} = 807 \text{ s}^{-1} (\pm 16)$  and  $K_{\text{M}} = 0.091 \text{ M} (\pm 0.003)$ , and  $k_{\text{cat}}/K_{\text{M}} = 8900 \text{ M}^{-1}\text{s}^{-1}$  (Figure 9, a), and for the system consisting of complex **2** and 5 equiv. of NaOH,  $k_{\text{cat}} = 190 \text{ s}^{-1} (\pm 4)$ ,  $K_{\text{M}} = 0.022 \text{ M} (\pm 0.001)$ , and  $k_{\text{cat}}/K_{\text{M}} = 8600 \text{ M}^{-1}\text{s}^{-1}$  (Figure 9, b). A comparison of the kinetic parameters for the two systems, **1** and 5 equiv. of NaOH and **2** and 5 equiv. of NaOH, shows that, in fact both of them have similar catalytic efficiency. The value of  $k_{\text{cat}}$ , the turnover efficiency of the complex **2** and 5 equiv. of NaOH system, is actually lower than the complex **1** and 5 equiv. of NaOH system, but this is compensated by the very low  $K_{\text{M}}$  value. Thus, the ratio  $k_{\text{cat}}/K_{\text{M}}$  becomes similar to that of complex **1** and 5 equiv. of NaOH. Apparently, the two complexes catalyze the reactions probably by different mechanisms, but ultimately reach similar catalytic efficiency. The nature of the mechanisms however, cannot be anticipated at the present moment. The complexes themselves, without addition of NaOH, also show good catalase activity (Table 5) but their Michaelis–Menten parameters could not be determined as they did not give saturation kinetics for the range of hydrogen peroxide concentrations studied.

### Spectroscopic Studies on the Catalyst Solution

Ligand field spectra of complex **1** taken during stepwise addition of NaOH show small but clear changes with three distinct isosbestic points at 310, 350 and 392 nm. On addition of 1 and 2 equiv. of NaOH, hardly any changes are observed in the spectrum of complex **1**. On addition of successive equivalents of NaOH (3–10 equiv.), the peaks at 330 nm start growing in intensity and the peaks at 357, 418 and 565 nm decrease in intensity. At 5 equiv. of NaOH added, the same trend continues, and no new clearly defined peaks are formed. On addition of more equivalents of NaOH, the peak at 330 nm is of high intensity,<sup>[19–21]</sup> and the spectrum from 400 to 700 nm appears as a broad tail going into the visible region. A brown precipitate appears concomitantly in the solution, indicating degradation of the complex.

A frozen solution EPR spectrum of a reaction mixture containing only complex **1** and hydrogen peroxide in ethanol taken 3 minutes after the addition of hydrogen peroxide (i.e. after the reaction has finished) shows a six-line signal typical of  $\text{Mn}^{\text{II}}$  ( $g = 2.01$ ,  $A = 90 \text{ G}$ ). No EPR signal can be detected, however, after the stepwise addition of NaOH to a solution of **1**, nor after the subsequent addition of hydrogen peroxide, suggesting that manganese(II) or mixed-

Table 5. Disproportionation of hydrogen peroxide by the three Mn–mesalim complexes (TON = Turnover number; moles of substrate molecules converted per mol of the catalyst)

Complexes <sup>[a]</sup>	TON in H <sub>2</sub> O <sub>2</sub> (without NaOH)	TON in H <sub>2</sub> O <sub>2</sub> (5 equiv. NaOH)	Conversion (%) (5 equiv. NaOH)
Mn(ClO <sub>4</sub> ) <sub>2</sub>	0 <sup>[b]</sup>	190 <sup>[b]</sup>	48%
[Mn <sub>2</sub> (etsalim) <sub>4</sub> (Hetsalim) <sub>2</sub> ](ClO <sub>4</sub> ) <sub>2</sub> (1)	180	3150 <sup>[c]</sup>	90%
[Mn(mesalim) <sub>2</sub> (OAc)(MeOH)] (2)	350	1810	91%
[Mn(mesalim) <sub>2</sub> Cl] (3)	270	1360	68%

<sup>[a]</sup> Reaction conditions: 1 mL of a 1 mM solution of the catalyst in methanol (2) or ethanol (1), H<sub>2</sub>O<sub>2</sub> = 2 mmol, room temp., turnovers after 3 min (catalyst/H<sub>2</sub>O<sub>2</sub> = 1:2000). <sup>[b]</sup> 5 mL of a 1 mM catalyst solution used (catalyst/H<sub>2</sub>O<sub>2</sub> = 1:400). <sup>[c]</sup> 3.5 mmol of H<sub>2</sub>O<sub>2</sub> used (catalyst/H<sub>2</sub>O<sub>2</sub> = 1:3500).

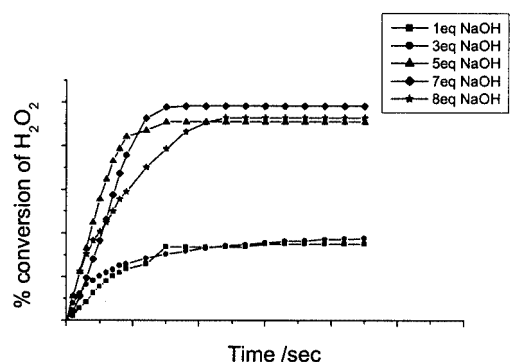


Figure 7. Conversion of H<sub>2</sub>O<sub>2</sub> vs. time, with successive amounts of NaOH added; catalyst = complex 1 (1 μmol) and 3.18 mmol of H<sub>2</sub>O<sub>2</sub> in 1 mL of ethanol

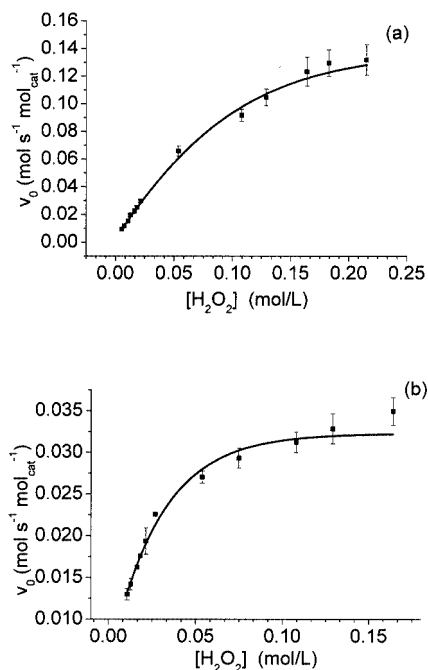


Figure 8. (a) Initial rate of substrate conversion versus substrate concentration at constant concentration of [Mn<sub>2</sub>(etsalim)<sub>4</sub>(Hetsalim)<sub>2</sub>](ClO<sub>4</sub>)<sub>2</sub> (1) + 5 equiv. NaOH in ethanol and (b) [Mn(mesalim)<sub>2</sub>(OAc)(MeOH)] (2) + 5 equiv. NaOH in methanol

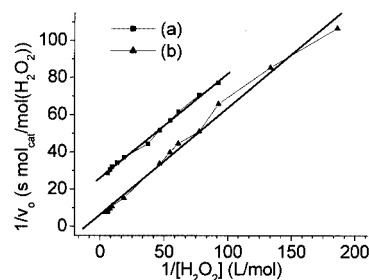


Figure 9. Lineweaver–Burk plot for (a) [Mn<sub>2</sub>(etsalim)<sub>4</sub>(Hetsalim)<sub>2</sub>](ClO<sub>4</sub>)<sub>2</sub> (1) + 5 equiv. NaOH in ethanol, and (b) [Mn(mesalim)<sub>2</sub>(OAc)(MeOH)] (2) + 5 equiv. NaOH in methanol

valent manganese(III)/(IV) species are not formed in this case.

Positive mode ESI-MS analysis was used to understand the nature of the species formed on addition of NaOH to a solution containing complex 1. To assist the assignment of peaks, the spectra were also measured from the solution of the complex prepared in [D<sub>6</sub>]ethanol (C<sub>2</sub>D<sub>5</sub>OD). Nondeuterated ethanol was used as the solvent for elution. A part of the complex ions undergo exchange with deuterated ethanol, and because of this, a pattern of lines with species ranging from nondeuterated, partly deuterated to completely deuterated complex ions can be observed. Analyzing the pattern of the peaks, it is clear that the ethoxy group on the ligand is rather labile, and in the metal complex it exchanges rapidly with the ethoxy group of the solvent ethanol, consistent with the earlier observation during complex synthesis (see above). Tables listing full details, relative intensities and assignments are available as Supporting Information.

A solution of complex 1 in ethanol exhibits peaks at 383.15 [Mn<sup>III</sup>(etsalim)<sub>2</sub>]<sup>+</sup>, 429.22 [Mn<sup>III</sup>(etsalim)<sub>2</sub>(EtOH)]<sup>+</sup>, 811.35 [Mn<sub>2</sub><sup>III</sup>(etsalim)<sub>4</sub>(EtOH)–H<sup>+</sup>]<sup>+</sup> and 865.30 {[Mn<sub>2</sub><sup>III</sup>(etsalim)<sub>4</sub>](ClO<sub>4</sub>)<sup>+</sup>. The presence of the latter two peaks suggests that the dinuclear core of the complex does persist in the solution. In deuterated ethanol the complex shows clusters of peaks at 383.15 [Mn<sup>III</sup>(etsalim)<sub>2</sub>]<sup>+</sup>, 388.19 [Mn<sup>III</sup>(etsalim)([D<sub>5</sub>]etsalim)]<sup>+</sup> and 393.19 [Mn<sup>III</sup>([D<sub>5</sub>]etsalim)<sub>2</sub>]<sup>+</sup> and at 429.23 [Mn<sup>III</sup>(etsalim)<sub>2</sub>(EtOH)]<sup>+</sup>, 434.26 [Mn<sup>III</sup>(etsalim)([D<sub>5</sub>]etsalim)(EtOH)]<sup>+</sup> and 439.29 [Mn<sup>III</sup>([D<sub>5</sub>]etsalim)<sub>2</sub>(EtOH)]<sup>+</sup>.

([D<sub>5</sub>]etsalim)<sub>2</sub>(EtOH)]<sup>+</sup>, as well as 5-line patterns for the dinuclear species in the ranges 811–831 and 865–885.

ESI-MS spectra of complex **1** and 5 equiv. of NaOH in ethanol reveal peaks at 451.26 {Na[Mn(etsalim)<sub>3</sub>(EtOH) – H<sup>+</sup>]}<sup>+</sup>, 497.28 {Na[Mn(etsalim)<sub>2</sub>(EtOH)<sub>2</sub> – H<sup>+</sup>]}<sup>+</sup>, 570.35 {Na[Mn(etsalim)<sub>3</sub>]}<sup>+</sup>, 787.47 {Na[Mn<sub>2</sub>(etsalim)<sub>4</sub> – 2 H<sup>+</sup>]}<sup>+</sup>, 833.46 {Na[Mn<sub>2</sub>(etsalim)<sub>4</sub>(EtOH) – H<sup>+</sup>]}<sup>+</sup>, 850.57 {Na[Mn<sub>2</sub>(etsalim)<sub>4</sub>(EtOH)(O)]<sup>+</sup>, and 952.57 {Na[Mn<sub>2</sub>(etsalim)<sub>5</sub> – H<sup>+</sup>]}<sup>+</sup>. The most interesting observation after addition of NaOH is the peak at 850.57, which is tentatively assigned to a dinuclear Mn–μ-oxo species. These assignments were all confirmed by the presence of the respective multi-line signals in the ESI-MS spectra with deuterated ethanol and NaOH in D<sub>2</sub>O. Furthermore, in the deuterated solvent a group of peaks of low intensity at 959–974 is observed, which could possibly be assigned to a di-μ-oxo species, {Na<sup>+</sup>[Mn<sup>IV</sup>(etsalim)<sub>4</sub>(EtOH)<sub>3</sub>(O)<sub>2</sub>]}<sup>+</sup>. However, this species was not observed in nondeuterated ethanol which unfortunately makes unambiguous assignment of these peaks not possible. Addition of hydrogen peroxide to this reaction mixture did not give rise any other peaks in the ESI-MS spectrum, as most of it was degraded before the active species could be measured.

### Discussion and Comparison to Other Systems

The  $k_{\text{cat}}$  and  $K_M$  values for the complexes **1** and **2** in combination with 5 equiv. of NaOH, can be compared to those of [Mn(bpia)(μ-OAc)<sub>2</sub>(ClO<sub>4</sub>)<sub>2</sub>] [bpia = bis(pyridylmethyl)(*N*-methylimidazol-2-ylmethyl)amine] which are  $k_{\text{cat}} = 1100 \text{ s}^{-1}$ ,  $K_M = 31.5 \text{ mM}$  and  $k_{\text{cat}}/K_M = 34000 \text{ M}^{-1}\text{s}^{-1}$ .<sup>[11]</sup> The present complex **1** or **2** and 5 equiv. of NaOH systems show the second best activity that has been reported until now for the manganese catalase mimics with the Mn(bpia) system in the first position. For the present studies, addition of a few equivalents of base was used successfully for increasing the catalase activity as has already been reported for other systems.<sup>[24]</sup> The rate acceleration on addition of NaOH possibly correlates with the availability of an intramolecular hydroxide for substrate deprotonation and with binding of the substrate at the bridging site between Mn ions in the reductive O–O bond-cleavage step.<sup>[24]</sup> After addition of NaOH, there might be μ-oxo or μ-hydroxo bond formation between the two manganese ions as is demonstrated by the use of sodium hydroxide for the syntheses of several μ-oxo-bridged, dinuclear manganese complexes.<sup>[26]</sup> For the [Mn(2-OH-salpn)<sub>2</sub>] ( $k_{\text{cat}} = 4.22 \text{ s}^{-1}$ ) and [Mn<sub>2</sub>(salpn)O<sub>2</sub>] ( $k_{\text{cat}} = 2500 \text{ s}^{-1}$ ) systems [salpn = *N,N'*-bis(salicylidene)-1,3-diaminopropane and 2-OH-salpn = *N,N'*-bis(salicylidene)-2-hydroxy-1,3-diaminopropane], the rate increases tremendously when the alkoxo-bridged dimer is replaced by a μ-oxo-bridged manganese dimer.<sup>[10]</sup> NaOH and *N*-methylimidazole were studied as bases in the catalase reaction with the manganese-mesalim and -etsalim complexes. Both bases increased the total conversion as well as the rate of the catalase reaction. The present system also gives higher catalytic efficiency than the recently reported [Mn<sub>2</sub>(L)<sub>2</sub>Cl<sub>2</sub>] system {L = 2-[bis(pyridin-2-ylmethyl)amino-methyl]-6-methoxyphenol}.<sup>[25]</sup>

The ligand field spectra recorded upon successive additions of NaOH indicate that the LMCT bands (300 nm and 360 nm) show clear changes with isosbestic points due to formation of one species from the original complex. Addition of more than 5 equiv. of NaOH results in formation of a precipitate, and the ligand field spectrum becomes broadened. ESI-MS analysis proved to be a useful tool for the interpretation of the species formed on addition of NaOH to the complex solution. The first role of NaOH may be to withdraw the proton on the imine nitrogen atom and thus make the complex more oxidizable. The removal of the proton from the imine nitrogen atom is evident from the peaks at 787.14 {Na<sup>+</sup>[Mn<sub>2</sub>(L)<sub>4</sub> – 2 H<sup>+</sup>]}<sup>+</sup> and at 833.18 {Na<sup>+</sup>[Mn<sub>2</sub>(L)<sub>4</sub>(EtOH) – 2 H<sup>+</sup>]} on addition of 5 equiv. of NaOH to the complex **1** solution, where both or at least one proton has to be withdrawn from the imine nitrogen atom on the etsalim ligand. The only species that could give a hint to the μ-oxo species formation was observed at 850.57, which could be assigned to a μ-oxo-bridged species with a relative intensity of 10%. Dinuclear Mn<sup>III</sup>/Mn<sup>III</sup> species have been proposed to be the active catalysts for H<sub>2</sub>O<sub>2</sub> disproportionation in several manganese catalases as well as functional catalase model complexes. X-band EPR spectra recorded at 77 K did not show the formation of a Mn<sup>IV</sup> species or a mixed-valent Mn<sup>II</sup>/Mn<sup>III</sup> or Mn<sup>III</sup>/Mn<sup>IV</sup> species, neither after addition of NaOH nor immediately after addition of hydrogen peroxide (i.e. during catalytic turnover). A brown precipitate that is insoluble in many solvents, characteristic of MnO<sub>2</sub>, is formed at the end of the reaction. Thus, the catalytically inactive species formed at the end of the reaction is probably due to the decomposition of the metal complex to form insoluble Mn<sup>IV</sup> oxides.

### Conclusion

In this study the synthesis, crystal structures, full characterization and catalase studies of three manganese complexes have been presented. It has been shown that complexes **1–3** in combination with 5–6 equiv. of NaOH show very high catalase activity and are only surpassed by the Mn–bpia system reported by Krebs and co-workers.<sup>[11]</sup> However, compared to the Mn–catalase enzyme, the  $k_{\text{cat}}$  value is still 20–30 times lower than the manganese–catalase enzymes and thus the catalytic efficiency ( $k_{\text{cat}}/K_M$ ) is still 200–300 times lower than that of the manganese–catalase enzymes. The turnover as well as the rate of the reaction increase remarkably with the addition of a few equivalents of NaOH to the catalyst solution. The complexes in combination with a few equivalents of sodium hydroxide (NaOH) are among the few catalase model systems that show turnover numbers up to 3000 in hydrogen peroxide disproportionation. ESI-MS analyses in deuterated solvents have been used to understand the nature of the active species formed on addition of 5 equiv. of NaOH. The exact nature of the active species participating

during turnover, however, could not be confirmed at the present moment.

## Experimental Section

**Physical Measurements:** UV/Vis/NIR measurements were performed with a Perkin–Elmer Lambda 900 UV/Vis/NIR spectrometer. IR spectra were recorded with a Perkin–Elmer FT-IR Paragon 1000 spectrometer.  $^1\text{H}$  NMR spectra were recorded with a Bruker 300 DPX MHz spectrometer. Elemental analyses were performed with a Perkin–Elmer series II CHNS/O analyzer 2400. EPR measurements were performed at 77 K using a Jeol Esprit RE-2X spectrometer with a Jeol Esprit 330 ESRE data system. EPR  $g$  values were determined relative to DPPH as an external “ $g$ -marker” ( $g = 2.0037$ ). Electrospray mass spectra were recorded with a Thermo Finnigan AQA apparatus. All solvents were of analytical grade and used without further purification unless stated otherwise.

**Catalase Activity:** Two different methods were carried out to get the turnover number,  $k_{\text{cat}}$ , the Michaelis constant,  $K_{\text{M}}$ , and  $k_{\text{cat}}/K_{\text{M}}$ . In the first experiment an aqueous solution of  $\text{H}_2\text{O}_2$  was added to a solution of the complex at room temperature. Dioxygen evolution was observed instantaneously and monitored manometrically. In a typical experiment, to find out the total conversion of dihydrogen peroxide,  $\text{H}_2\text{O}_2$  (2 mmol, 2000 equiv., 0.17 mL of a 35% aqueous solution) was added to the complex (1 mL of a 1 mM solution in EtOH for **2** and in MeOH for **1** and **3**) at room temperature. Dioxygen evolution was observed instantaneously and monitored manometrically. Initial rate measurements were performed by plotting the volume of dioxygen evolved versus time in seconds.

**Kinetic Measurements:** In the second experiment, for the kinetic studies, an optical oxygen sensor was used to measure the initial rates of the  $\text{H}_2\text{O}_2$  decomposition. The complex was added to an aqueous  $\text{H}_2\text{O}_2$  solution of increasing concentration and the initial rate was recorded. The data were fitted into the Michaelis–Menten equation, and the turnover number,  $k_{\text{cat}}$ , the Michaelis constant,  $K_{\text{M}}$ , and  $k_{\text{cat}}/K_{\text{M}}$  were determined from the double reciprocal Lineweaver–Burk plot (Figure 9).  $K_{\text{M}}$  is a criterion for substrate affinity, the turnover number,  $k_{\text{cat}}$ , can be interpreted as the rate of substrate conversion into the corresponding products and  $k_{\text{cat}}/K_{\text{M}}$  is a criterion for catalytic efficiency.

**Syntheses: Caution:** Perchlorate salts are potentially explosive and should be handled with appropriate care! The following abbreviations are used throughout the text: Hmesalim = methyl salicylimidate, Hetsalim = ethyl salicylimidate. All reagents and solvents were used as received with no attempt to remove water or molecular oxygen. The ligand Hmesalim was synthesized according to a published procedure.<sup>[16,27,28]</sup>

**[Mn<sub>2</sub>(etsalim)<sub>4</sub>(Hetsalim)<sub>2</sub>](ClO<sub>4</sub>)<sub>2</sub> (1):** The ligand Hmesalim (0.2 g, 1.32 mmol) was dissolved in absolute EtOH (10 mL). Manganese(II) perchlorate (0.108 g, 0.44 mmol) was added to the solution. The solution was stirred for 15 min and filtered. Green crystals were obtained after a few days by layering the reaction mixture with diethyl ether and hexane. Yield of crude product: 55% (0.156 g). UV/Vis ( $\text{CH}_3\text{CN}$ ):  $\lambda_{\text{max}}$ . ( $\epsilon$  [ $\text{M}^{-1}\text{cm}^{-1}$ ]) = 304 ( $38 \times 10^3$ ), 357 ( $20 \times 10^3$ ), 418 (2400), 565 (400), 971 (76) nm. IR (diamond):  $\tilde{\nu} = 3268$  (m), 1606 (s), 1588 (s), 1455 (s), 1399 (s), 1214 (m), 1088 (vs), 959 (m), 868 (m), 758 (s), 618 (s), 523 (s), 427 (s)  $\text{cm}^{-1}$ .  $\text{C}_{27}\text{H}_{31}\text{ClMnN}_3\text{O}_{10}$  (1295.88): calcd. C 50.05, H 4.82, N 6.4; found C 50.0, H 5.07, N 6.67.  $\mu_{\text{B}} = 4.8$  BM per manganese(III). MS (ESI):

$m/z = 383$  [ $\text{Mn}^{\text{III}}(\text{etsalim})_2$ ] $^+$ , 429.22 [ $\text{Mn}(\text{etsalim})_2(\text{EtOH})$ ] $^+$ , 811.35 [ $\text{Mn}_2(\text{etsalim})_4(\text{EtOH}) - \text{H}^+$ ] $^+$ , 865.30 [ $\text{Mn}_2^{\text{III}}(\text{etsalim})_4(\text{ClO}_4)$ ] $^+$ .

**[Mn(mesalim)<sub>2</sub>(OAc)(MeOH)·MeOH (2):** The ligand Hmesalim (1.85 g, 12.25 mmol) was dissolved in absolute MeOH (10 mL). Manganese(II) acetate (1 g, 4.08 mmol) was added to the solution, and the solution was stirred for 15 min. Then diethyl ether (20 mL) was added to the solution, and again the reaction mixture was stirred for 15 min. The solution was filtered, and crystals were grown in a few days by layering the MeOH/ether solution with hexane. Yield of crude product: 61.5% (1.2 g) UV/Vis ( $\text{CH}_3\text{CN}$ ):  $\lambda_{\text{max}}$ . ( $\epsilon$  [ $\text{M}^{-1}\text{cm}^{-1}$ ]) = 304 ( $16 \times 10^3$ ), 353 ( $9 \times 10^3$ ), 411 (1860), 562 (277) nm. IR (diamond):  $\tilde{\nu} = 3446$  (m), 3167 (m), 1609 (s), 1590 (s), 1542 (vs), 1452 (s), 1412 (s), 1330 (m), 1231 (vs), 1158 (s), 1098 (s), 863 (s), 748 (s), 626 (s), 492 (s)  $\text{cm}^{-1}$ .  $\text{C}_{19}\text{H}_{23}\text{MnN}_2\text{O}_7 \cdot 2\text{MeOH}$  (510.42): calcd. C 49.42, H 6.12, N 5.49; found C 49.12, H 6.51, N 5.86.  $\mu_{\text{B}} = 4.6$  BM. MS (ESI):  $m/z = 354.5$  [ $\text{Mn}^{\text{III}}(\text{mesalim})_2$ ] $^+$ , 415 {[ $\text{Mn}(\text{mesalim})_2(\text{OAc})$ ] +  $\text{H}^+$ ] $^+$ , 447 {[ $\text{Mn}(\text{mesalim})_2(\text{OAc})(\text{MeOH})$ ] +  $\text{H}^+$ ] $^+$  and 506 {[ $\text{Mn}(\text{mesalim})_3$ ] +  $\text{H}^+$ ] $^+$ .

**X-ray Crystallographic Study:** Intensity data for single crystals of **1** and **2** were collected at 150 K using graphite-monochromated  $\text{Mo-K}_\alpha$  radiation, with a Nonius Kappa CCD diffractometer on rotating anode. A correction for absorption was considered unnecessary in the case of **1**. For **2**, a multi-scan absorption correction was applied using PLATON/MULABS (0.678–0.903 transmission range).<sup>[29]</sup> The structures were solved by direct methods using SHELXS-97<sup>[30]</sup> (**1**) or SIR97<sup>[31]</sup> (**2**), and refined on  $F^2$  using SHELXL-97.<sup>[30]</sup> All non-hydrogen atoms were refined with anisotropic displacement parameters. All hydrogen atoms, and in particular those attached to nitrogen and oxygen atoms, were positively identified in a difference Fourier map. The position of the hydroxy hydrogen atom of the coordinated methanol molecule in **2** was refined with a restraint on the O–H distance. All other hydrogen atoms were constrained to idealized geometries and allowed to ride on their carrier atoms. All hydrogen atoms were refined with an isotropic displacement parameter related to the equivalent displacement parameter of their carrier atoms. Structure validation and preparation of molecular graphics were performed with the PLATON package.<sup>[29]</sup> CCDC-244114 (**1**) and -244115 (**2**) contain the supplementary crystallographic data for this paper. These data can be obtained free of charge at [www.ccdc.cam.ac.uk/contents/retrieving.html](http://www.ccdc.cam.ac.uk/contents/retrieving.html) [or from the Cambridge Crystallographic Data Centre, 12 Union Road, Cambridge CB2 1EZ, UK; Fax: (internat.) +44-1223-336-033; E-mail: [deposit@ccdc.cam.ac.uk](mailto:deposit@ccdc.cam.ac.uk)].

## Acknowledgments

This work has been carried out within the framework of the Council for Chemical Sciences of the Netherlands Foundation for Scientific Research (CW-NWO), through a grant from the special program “Aspasia”. Financial support by the DFG (Deutsche Forschungsgemeinschaft, SPP 1118) is gratefully acknowledged. The authors thank Prof. Dr. Jan Reedijk for stimulating discussions. We thank one of the referees for useful suggestions.

[1] J. Reedijk, E. Bouwman, *Bioinorganic catalysis*, Marcel Dekker Inc., New York, 1999.

[2] G. C. Dismukes, in *Bioinorganic catalysis* (Ed.: J. Reedijk), Marcel Dekker, New York, 1993, pp. 317–346.

- [3] Y. Kono, I. Fridovich, *J. Biol. Chem.* **1983**, 258, 3646–3648.
- [4] I. Michaud-Soret, L. Jacquamet, N. Debaecker-Petit, L. Le Pape, V. V. Barynin, J. M. Latour, *Inorg. Chem.* **1998**, 37, 3874–3876.
- [5] G. S. Allgood, J. J. Perry, *J. Bacteriol.* **1986**, 168, 563–567.
- [6] J. Penner-Hahn, *Manganese Redox Enzymes*, VCH Publishers, New York, **1992**.
- [7] L. Dubois, F. Caspar, L. Jacquamet, P. E. Petit, M. F. Charlot, C. Baffert, M. N. Collomb, A. Deronzier, J. M. Latour, *Inorg. Chem.* **2003**, 42, 4817–4827.
- [8] P. J. Pessiki, G. C. Dismukes, *J. Am. Chem. Soc.* **1994**, 116, 898–903.
- [9] L. Dubois, D. F. Xiang, X. S. Tan, J. Pecaut, P. Jones, S. Baudron, L. Le Pape, J. M. Latour, C. Baffert, S. Chardon-Noblat, M. N. Collomb, A. Deronzier, *Inorg. Chem.* **2003**, 42, 750–760.
- [10] A. Gelasco, S. Bensiek, V. L. Pecoraro, *Inorg. Chem.* **1998**, 37, 3301–3309.
- [11] M. U. Triller, W. Y. Hsieh, V. L. Pecoraro, A. Rompel, B. Krebs, *Inorg. Chem.* **2002**, 41, 5544–5554.
- [12] T. Katsuki, *Coord. Chem. Rev.* **1995**, 140, 189–214.
- [13] A. Gelasco, A. Askenas, V. L. Pecoraro, *Inorg. Chem.* **1996**, 35, 1419–1420.
- [14] A. Gelasco, V. L. Pecoraro, *J. Am. Chem. Soc.* **1993**, 115, 7928–7929.
- [15] M. D. Godbole, E. Grigiotti, P. Zanello, A. M. Mills, A. L. Spek, E. Bouwman, *Inorg. Chim. Acta*, in press.
- [16] D. S. C. Black, M. J. Wade, *Aust. J. Chem.* **1972**, 25, 1797–1810.
- [17] M. D. Godbole, O. S. Roubeau, A. M. Mills, H. Kooijman, E. Bouwman, manuscript in preparation.
- [18] H. L. Shyu, H. H. Wei, Y. Wang, *Inorg. Chim. Acta* **1999**, 290, 8–13.
- [19] L. J. Boucher, V. W. Day, *Inorg. Chem.* **1977**, 16, 1360–1367.
- [20] M. Marappan, V. Narayanan, M. Kandaswamy, *J. Chem. Soc., Dalton Trans.* **1998**, 3405–3409.
- [21] A. Neves, S. M. D. Erthal, I. Vencato, A. S. Ceccato, Y. P. Mascarenhas, O. R. Nascimento, M. Horner, A. A. Batista, *Inorg. Chem.* **1992**, 31, 4749–4755.
- [22] K. Wiegardt, U. Bossek, D. Ventur, J. Weiss, *J. Chem. Soc., Chem. Commun.* **1985**, 347–349.
- [23] M. M. Whittaker, V. V. Barynin, S. V. Antonyuk, J. Whittaker, *Biochemistry* **1999**, 38, 9126–9136.
- [24] A. E. M. Boelrijk, G. C. Dismukes, *Inorg. Chem.* **2000**, 39, 3020–3028.
- [25] N. Reddig, D. Pursche, M. Kloskowski, C. Slinn, S. M. Baldeau, A. Rompel, *Eur. J. Inorg. Chem.* **2004**, 879–887.
- [26] M. Maneiro, M. R. Bermejo, R. Fondo, A. M. Gonzalez, J. Sanmartin, J. C. Garcia-Monteagudo, R. G. Pritchard, A. M. Tyryshkin, *Polyhedron* **2001**, 20, 711–719.
- [27] P. Stoss, *Chem. Ber.* **1978**, 111, 314–319.
- [28] P. Vinkler, K. Thimm, J. Vob, *Justus Liebigs Ann. Chem.* **1976**, 1976, 2083–2093.
- [29] A. L. Spek, *J. Appl. Crystallogr.* **2003**, 36, 7–13.
- [30] G. M. Sheldrick, University of Göttingen, Göttingen, Germany, **1997**.
- [31] A. Altomare, M. C. Burla, M. Camalli, G. L. Cascarano, C. Giacovazzo, A. Guagliardi, A. G. G. Moliterni, G. Polidori, R. Spagna, *J. Appl. Crystallogr.* **1999**, 32, 115–119.

Received July 16, 2004

Early View Article

Published Online November 24, 2004